



Original Research Article

Analysis of real-time multi channel microelectrode recordings of rats: A study with computational simulation

V Rama Raju^{1,2,3,*}

¹CMR College of Engineering & Technology, Medchal Road, Kandlakoya,, Hyderabad, Telangana, India

²Nizam's Institute of Medical Sciences, Hyderabad, Telangana, India

³CMR Institute of Medical Sciences, Medchal Road, Kandlakoya,, Hyderabad, Telangana, India



ARTICLE INFO

Article history:

Received 24-02-2022

Accepted 19-04-2022

Available online 10-06-2022

Keywords:

Burst-spike-detection

Collision-test

Elastic-template

Hierarchical-clustering

Multi channel recording

ABSTRACT

This study discuss the analysis of a real-time multi channel microelectrode recordings of rats with computational simulation and mathematical statistical modeling's. If the impedance-of every site of neuro-sensor, i.e., electrode is fairly at a low level as well as the gap between sensor-sites is applicably very minute, a spike-generated and also computed by a neuron is asynchronously/concurrently gathered at multi neuro-sensor/electrode locations in conjunction with distinct stimulus-intensities, i.e., amplitudes (strength of the signals).

This is an Open Access (OA) journal, and articles are distributed under the terms of the [Creative Commons Attribution-NonCommercial-ShareAlike 4.0 License](https://creativecommons.org/licenses/by-nc-sa/4.0/), which allows others to remix, tweak, and build upon the work non-commercially, as long as appropriate credit is given and the new creations are licensed under the identical terms.

For reprints contact: reprint@ipinnovative.com

1. Introduction

Split of signal-spikes computer simulated-generated adjoining-neurons is a key problem in extra cellular micro electrode signal-recording from cell-dense-areas of the animal-brain (for instance, hippo-cmapul pyra midal cells). Even though we have different types of software, hardware, firmware windowing-spectral minimization methods, the number of neural cells distinguishable as of single unit single channel signal recordings is small, be in the region of two.¹ Normal standard-procedures can not be distinguished amongst analogous- stimulus-amplitudes/spikes initiating as of or on/ or after distinct-neurons intermediate as of the stimulating-sensor and acquiring micro electrode.² However, while latest multi channel spikes/data is to be grouped for clustering purposes, such technique needs the effect of preceding, ie.,eralier clustering-of-spike-data gathered under identical-conditions (the identical-electrode, multi neuronal locations, etc.). Such type of necessity

enforces and necessitates the constraints or restrictions on the applicability-of the technique to a range-of multi channel spikes-data.

Therefore, we suggest at this juncture a significant enhancement of the stereo trode technique applying through the co-variance, instead of simply the peak-amplitude-ratio, amongst a pattern-tmplate/signature plus a definite spike-acquired by using a multi site micro electrode.³

2. Goal

To explore the multi unit multi site micro electrode signal acquisitions of rats hippocampus pyramidal cell layers as well as deep-brain stimulation in anesthetized non-primate-animals using artificial intelligence/machine-learning-techniques (both supervised and unsupervised), signal, as well as clustering-methods..

3. Methods

Standard traditional windowing-methods distinguish neuronal-spikes by means of referencing their highest-

* Corresponding author.

E-mail address: drvrr@cmrcet.ac.in (V. R. Raju).

signal-amplitudes primarily. Though, limitations of spike-stimulus-amplitudes in the middle of numerous-cells-neurons are complicated to ascertain, e.g., two neural-cells/neurons which are intermediate after the sensor-site might have virtually indistinguishable stimulus-amplitudes/signal-strengths or power of the signal. Mc Naughton, et.al. established the stereo trode technique wherein neuronal-spikes are divided by referring to the probabilistic joint-distribution of highest/peak-amplitudes values achieved by multi channel signal recordings.² The following Figure 1 depicts is derived which is a combination of signal-decompositin/.

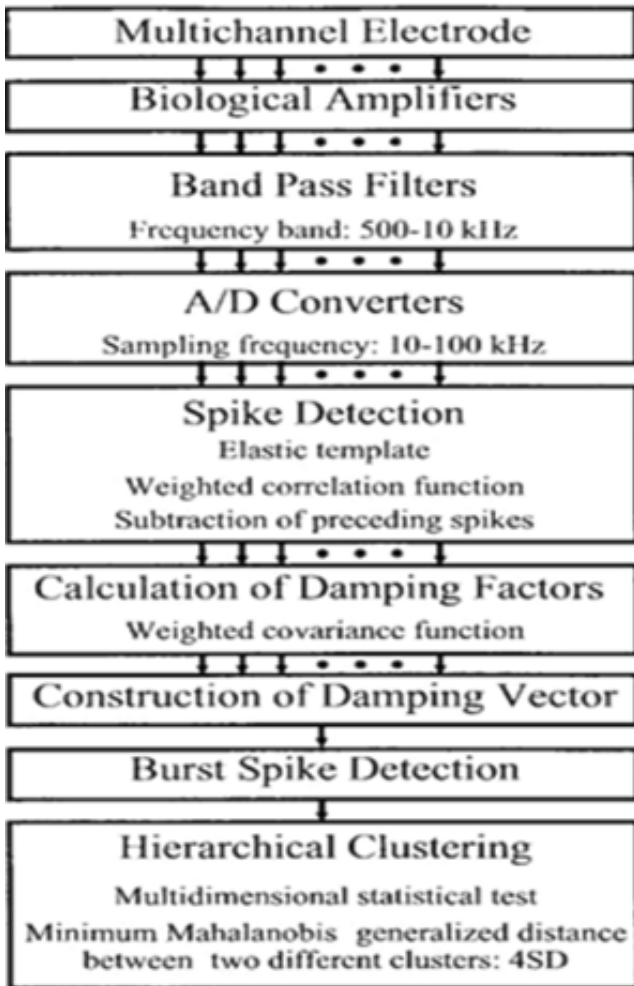


Fig. 1: Segmentation of the data

4. Idea

If a succulently strong stimulus is applied to whatsoever part of our or animal body then it gives rise to some excitation and this excitation is due to ion permeability of the membranes. i.e., fluctuations in the membranes. The electrical-action potentials of the aimed neuron is acquired

extra cellularly in conjunction with a multi site micro electrode (Figure 2).

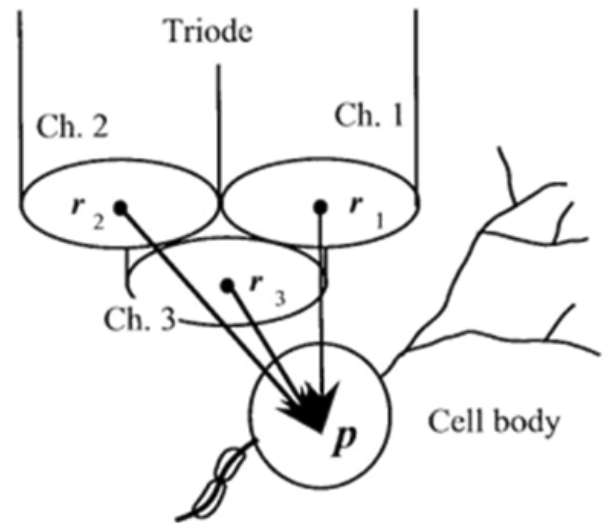


Fig. 2: Simulated Electrode

Let us consider a spike-generated at the length of time "T" passing through the aimed neural-cell/ the-neuron positioned at a 'point' "p" is derived as

$$v_n(t) = h(t, p - r_n) \times w(t - T) \dots\dots (1)$$

By way of focussing on the mitigation/ effect of the spatial (temporal) damping factor, the equation (1) is converted in to the

$$v_n(t) = h(p - r_n) \cdot w(t - T) + \epsilon_n(t) \dots\dots(2)$$

By means of minimizing the energy of the error-function, is projected as and then the equation

$$v_n(t) \cong h(p - r_n) \cdot w(t - T) \dots\dots(3)$$

is normalized so that its negative roughly equalizes the -Vepeak of signal-amplitude of evry neural-spikes.

$$\hat{H}(p) = (\hat{h}(p-r_1), \hat{h}(p-r_2), \hat{h}(p-r_3), \dots, \hat{h}(p-r_N)) \quad (4)$$

⁴, template-signal/wave forms ought be carefully-chosen, contemplating the range of examined spike of the signal-waveforms⁵.

Based-on the unique-template, elastic-template

$$\text{is derived as } w^\gamma = \psi(t/\gamma) \dots\dots\dots(5)$$

where indicates the duration ratio of to i.e., the resistance of is described by the optimum value of is determined so that each spike detected has a maximum-correlation with optimized

5. Identifying the spikes

Thecorrelation-technique has been extensively applied for identifying neural/neuronal-spikes.⁴ In this, the acquired-signals-having high-correlation-coefficients in conjunction through a pattern-matching-template are identified as signal-amplitudes-spikes.⁴⁻⁷

The following Figure 3 shows one of the correlation-coefficients-whenexceeds, a amplitude of the signal-spike is

believed to have been identified.

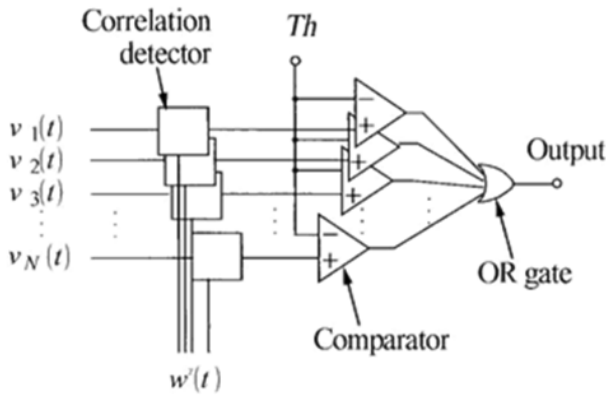


Fig. 3:

5.1. Correlation—coefficient computation

To enhance detection of the signal spikes of waveforms, the weight -v e c t o r f u n c t o r can be used for computation of the c o r r e l a t i o n - c o e f f i c i e n t s. Consequently, by employing the weight functors, the processed—signal at the n - t h e l e c t r o d e - p o i n t $w_n(t)$ comprises analogous overlap and correlating-spikes

$$v_n = \sum_{j=-\infty}^{+\infty} v_{j, n}(t) \dots \dots \dots (6)$$

Where in, $v_{j, n}(t)$ yielding the j-th interpreted spike formed through some neuronal cells inside the region of the n - t h e l e c t r o d e - p o i n t at T_i time T_i . Consequently, conceived that the weight- functor $W^\gamma(t)$ attenuate the neural-signal-spikes happening beforehand plus following the neural-spike witnessed at , by means of neuronal-spike duration-ratio ‘’. Here, we applied a smoothed-square-waveform of the elastic-template for weighting

$$w^\gamma(t) = \frac{\int_{-\frac{\delta}{2}}^{+\frac{\delta}{2}} w^\gamma(t+\tau)^2 d\tau}{\int_{-\frac{\delta}{2}}^{+\frac{\delta}{2}} w^\gamma(\tau)^2 d\tau} \dots \dots \dots (7)$$

i.e.,

$$W^\gamma(t) = \frac{\int_{-\frac{\delta}{2}}^{+\frac{\delta}{2}} w^\gamma(t^2+\tau^2+2t\tau) d\tau}{\int_{-\frac{\delta}{2}}^{+\frac{\delta}{2}} w^\gamma(\tau)^2 d\tau} \dots \dots \dots (8)$$

δ -showing the length of the period of the neural-spike-train that is 1 ± 3 milli-seconds. (± 1 mil Second to ± 3 mil Seconds). Through this weighting- vector allowing us to separate the neural/neuronal-spike observed at T_k as given in the following expression (9)

$$v_{k,n}(t) \cong v_n(t) \cdot W^\gamma(t-T_k) \dots \dots \dots (9)$$

Thus, can change the pattern/signature -signal pattern-template as

$$w^\gamma(t) \cong w^\gamma(t) \cdot W^\gamma(t - T_k) \dots \dots \dots (10)$$

We can now thus can generate/compute the correlation coefficient concerning $v_{k,n}(t)$ as well as the pattern-template (i.e.,the variable-template) as

$$R_{k,n}^\gamma(t) = \frac{\int_{-\delta}^{+\delta} v_{k,n}(t+\tau) \cdot w^\gamma(\tau) d\tau}{\sqrt{\int_{-\delta}^{+\delta} v_{k,n}(t+\tau)^2 dT \cdot \int_{-\delta}^{+\delta} w^\gamma(\tau)^2 d\tau}} \dots \dots \dots (11)$$

By changing the expression (11) into the expression (12) through the application of expression (9), as proved in the equation shown below

$$R_{k,n}^\gamma \cong \frac{\int_{-\delta}^{+\delta} v_n(t+\tau) \cdot w^\gamma(t+\tau-Tk) \cdot w^\gamma(\tau) \cdot W^\gamma(\tau) d\tau}{\sqrt{\int_{-\delta}^{+\delta} v_n(t+\tau)^2 \cdot W^\gamma(t+\tau-Tk)^2 d\tau \cdot \int_{-\delta}^{+\delta} w^\gamma(\tau)^2 \cdot W^\gamma(\tau)^2 d\tau}}$$

$$R_{k,n}^\gamma$$

$$\cong \frac{\int_{-\delta}^{+\delta} v_n(Tk+t) \cdot w^{\gamma k}(T) \cdot w^\gamma(\tau) \cdot W^{\gamma k}(\tau)^2 d\tau}{\sqrt{\int_{-\delta}^{+\delta} v_n(Tk+t)^2 \cdot W^{\gamma k}(\tau)^2 dT \cdot \int_{-\delta}^{+\delta} w^{\gamma k}(\tau)^2 \cdot W^{\gamma k}(\tau)^2 d\tau}}$$

$$R_n^\gamma$$

$$= \frac{\int_{-\delta}^{+\delta} v_n(t+\tau) \cdot w^\gamma(\tau) \cdot W^\gamma(\tau)^2 d\tau}{\sqrt{\int_{-\delta}^{+\delta} v_n(t+\tau)^2 \cdot W^\gamma(\tau)^2 dT \cdot \int_{-\delta}^{+\delta} w^\gamma(\tau)^2 \cdot W^\gamma(\tau)^2 d\tau}}$$

$$R_{k,n}^{\gamma k}(T_k) \cong R_n^{\gamma k}(T_k) \dots \dots \dots (15)$$

$$v_n^{(k)}(t) = \sum_{j \geq k}^{+\infty} v_{j,n}(t) = v_n(t) - \sum_{j=-\infty}^{k-1} v_{j,n}(t) \cong v_n(t) - \sum_{j \geq k}^{+\infty} \hat{h}(p_j - r_n) \cdot w^{\gamma j}(t-T_{j,n}) \dots \dots \dots (16)$$

By connecting the $v_n^{(k)}(t)$ as $v_n(t)$ in equation (14), the k-th neural-spike is characterized or distinguished from $v_n^{(k)}(t)$ unaltered through positive (+Ve) deflections or refractions of previous train neural-spikes.

5.2. Damping factorial generation

Through the application of estimating functor

$$E_n(T_{kn}) = \frac{1}{2\delta} \int_{-\delta}^{+\delta} \varepsilon((T_{kn} + \tau)^2) d\tau$$

$$= \frac{1}{2\delta} \int_{-\delta}^{+\delta} \varepsilon \left(v_{k,n}(T_{k,n} + \tau) - h(P_k - r_n) \cdot w^{\gamma_j}(\tau) \right)^2 d\tau$$

.....(17)

Then the equation yield

$$\frac{dE_n(T_{k,n})}{dh(P_k - r_n)} = - \frac{1}{2\delta} \int_{-\delta}^{+\delta} 2 \left(v_{k,n}(T_{k,n} + T) - h(P_k - r_n) \cdot w^{\gamma_j}(\tau) \right) \cdot w^{\gamma_j}(\tau) d\tau$$

.....(18)

$$v_{k,n}(T_{k,n} + T) - h(P_k - r_n) \cdot w^{\gamma_j}(T)$$

$$= - \frac{1}{2\delta} \int_{-\delta}^{+\delta} 2 \left(v_{k,n}(T_{k,n} + \tau) \cdot W^{\gamma_k}(\tau) - h(P_k - r_n) \cdot w^{\gamma_j}(\tau) W^{\gamma_k}(\tau) \right) d\tau$$

.....(19)

And then the above expression, i.e., (19) can be computed and while computing it must be set to

$$\widehat{h}(P_k - r_n)$$

$$\therefore \widehat{h}(P_k - r_n) \cong \frac{\int_{-\delta}^{+\delta} v_{k,n}(T_{k,n} + \tau) \cdot W^{\gamma_k}(\tau) \cdot W^{\gamma_k}(\tau)^2 d\tau}{\int_{-\delta}^{+\delta} w^{\gamma_k}(\tau)^2 \cdot W^{\gamma_k}(\tau)^2 d\tau} = \widehat{h}(P_k - r_n) \dots (20)$$

Hence, it is set to $\widehat{h}(P_k - r_n)$

Now, if $\int_{-\delta}^{+\delta} w^{\gamma_k}(\tau)^2 d\tau = 1$, the expression (20) is identically equal to the covariance between $v_n(T_{k,n} + t)$ and also $w^{\gamma_k}(\tau)$.

6. Spike train potentials

A pair-of-spikes is measured to happen in a gust-under the subsequent constraints: the inter-spike/interval (I S I) is $I S I_{b_min}, ISI_{b_max}$, the corr-coefficient of damping-vectors is $(C.C.b_min, 1)$ and attenuation ratio-of-spike amplitudes/signal-strengths ar $(attnb_min, attnb_max)$ which is depicted in the following Figure 4.

7. Conglomerate-clustering

The cluster is considered as a normal-distribution of $N(H; \mu_i, \Sigma_i)$:

$$N(H; \mu_i, \Sigma_i) = \frac{1}{(\sqrt{2\pi})^2 \sqrt{\Sigma_i}} e^{-\frac{1}{2}(H - \mu_i)^T \Sigma_i^{-1} (H - \mu_i)} \dots (21)$$

$$P_{i,j} \cong (1/2)^i$$

$$P_{i,j} \cong (1/2)^i \left[\int_{|I_{\mu_i - H}| > |\mu_j - H|} N(H; \mu_i, \Sigma_{i,j}) dH + \int_{|I_{\mu_i - H}| > |\mu_j - H|} N(H; \mu_i, \Sigma_{i,j}) dH \right]$$

$$\int_{-\infty}^{\infty} \sqrt{\left(\frac{1}{2}(\mu_i - \mu_j)\right)^T \Sigma_{i,j}^{-1} \left(\frac{1}{2}(\mu_i - \mu_j)\right)} N(h; 0, 1) dh \cong \int_{-\infty}^{\infty} \sqrt{\left(\frac{1}{2}(\mu_i - \mu_j)\right)^T (\mu_i - \mu_j)^{-1} \Sigma_{i,j}^{-1} (\mu_i - \mu_j)} N(h; 0, 1) dh$$

.....(22)

$$(\mu_i - \mu_j)^T \left(\frac{1}{2}\right) (\Sigma_i + \Sigma_j)^{-1} \leq 4$$

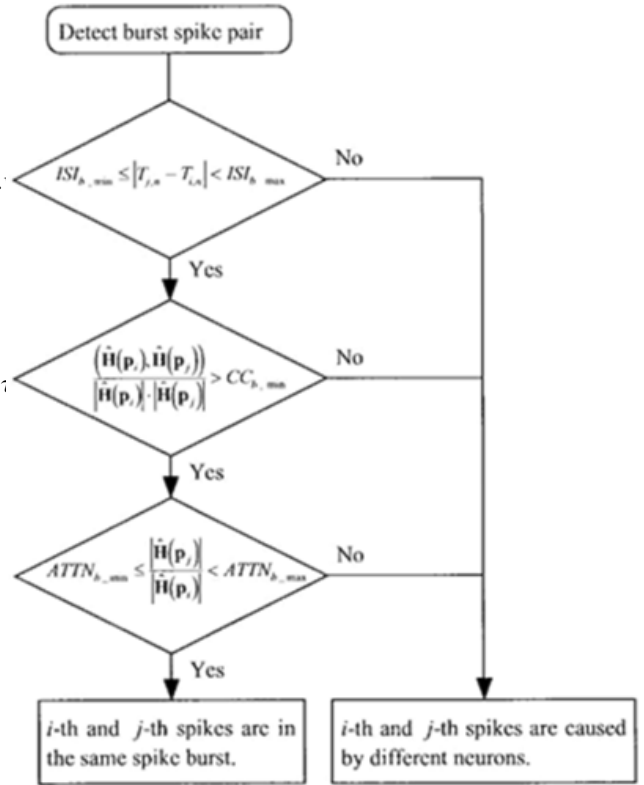


Fig. 4: ata and System flow for the spikes-pairs discovery into a spike-burst. ⁸⁻¹¹

8. Acquisition of spikes-data

A triode/ or a 7 – core - electrode was employed as a multi-site-electrode which consists of a pack of 3 fine stainless-steel-wires (Figure 2 ; 50μ-diameter, ~50k -impedance at 1kilo-Hz). The cross section of each wire was employed as the detection area-of-neuronal activity. The 7-core-electrode was a quartz-coated-electrode through 7-core-platinum/tungsten (⁹⁰/₁₀) cores (Figure 5, 1±2Meg -impedance at a 1kilo Hz).

9. Results and Discussion

This study discussed the equality of a clusters/group with a hippo-campus neuronal or neural-cells. But, the rationality of this conception has not yet resolute. We skilled additional supplementary explorations in which the targeted neuron was distinguished by the collision test. The damping-vectors were resolute by our grouping technique. Subsequently the damping-vectors of the perceived neuronals neuron/neural-cell distilled in a clustering-group that interconnected thriving to one of the cluster/groups in the multi-cluster/group distribution, representing the neuron-cluster communication.

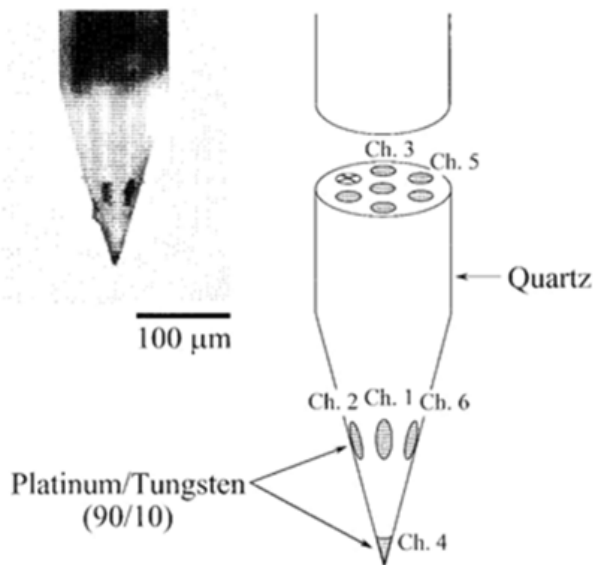


Fig. 5: Photo micro graph followed by the illustration of a 7-core – neuro-electrode. The core through an X is a non-functional-site.

10. Conclusion

The computational simulation and statistical modeling helps a lot in medical diagnosis especially for effective medical diagnostics in connection with the Brain disease and disorders like Parkinson's disease, Alzheimer's, cancer malignancy. So the developed simulation procedure for asynchronously classifying many neural-spikes and neuronal-spikes as of multi site multi-real time channelographs of the rats-brain. This simulated technique is more effective and more efficient in investigating multi neural connections in nearby linked neuronal networks.

11. Conflict of Interest

The researcher claims no conflict of interest.

12. Source of Funding

None.

References

1. Park K. Clinical outcome prediction from analysis of microelectrode recordings using deep learning in subthalamic deep brain stimulation for Parkinson's disease. *Plos One*. 2021;16(1):e0244133. doi:10.1371/journal.pone.0244133.
2. Koirala N. Acquisition of MER Data of NEURON neurons with deep brain stimulation in Parkinson's. *Scientific Reports*. 2020;10:1–13.
3. Barbe MT, Dembek TA, Becker J, Raethjen J, Hartinger M, Meister IG, et al. Individualized current-shaping reduces DBS-induced dysarthria in patients with essential tremor. *Neurology*. 2014;82(7):614–9. doi:10.1212/WNL.000000000000127.
4. Barbe MT. Multiple source current steering—a novel deep brain stimulation concept for customized programming in a Parkinson's disease patient. *Park Relat Disord*. 2014;20(4):471–3. doi:10.1016/j.parkreldis.2013.07.021.
5. Berenstein C, Mens LHM, Mulder JJS, Vanpoucke FJ. Current steering and current focusing in cochlear implants: comparison of monopolar, tripolar, and virtual channel electrode configurations. *Ear Hear*. 2008;29(2):250–60. doi:10.1097/aud.0b013e3181645336.
6. Blomstedt P. Deep brain stimulation in the posterior subthalamic area in the treatment of essential tremor. *Mov Disord*. 2016;25(10):1350–6. doi:10.1016/j.hears.2008.03.006.
7. Bonham BH, Litvak LM. Current focusing and steering: Modeling, physiology, and psychophysics. *Hear Res*. 2008;242(1-2):141–53. doi:10.1016/j.hears.2008.03.006.
8. Bour LJ, Lourens MAJ, Verhagen R, de Bie R, van den Munckhof P, Schuurman P, et al. Directional Recording of Subthalamic Spectral Power Densities in Parkinson's Disease and the Effect of Steering Deep Brain Stimulation. *Brain Stimulati*. 2015;8(4):730–41. doi:10.1016/j.brs.2015.02.002.
9. Breiman L. Random Forests. *Mach Learn*. 2001;45:5–32. doi:10.1023/A:1010933404324.
10. Buhlmann J, Hofmann L, Tass PA, Hauptmann C. Modeling of a segmented electrode for desynchronizing deep brain stimulation. *Front Neuroeng*. 2011;4:15. doi:10.3389/fneng.2011.00015.
11. Butson C, Cooper SE, Henderson JM, McIntyre CC. Patient-specific analysis of the volume of tissue activated during deep brain stimulation. *Neuroimage*. 2007;34(2):661–70.

Author biography

V Rama Raju, Professor

Cite this article: Raju VR. Analysis of real-time multi channel microelectrode recordings of rats: A study with computational simulation. *IP Indian J Neurosci* 2022;8(2):125-129.